Journal of The Electrochemical Society, **157** (6) D370-D375 (2010)
0013-4651/2010/157(6)/D370/6/$28.00 © The Electrochemical Society

Influence of Citric and Ascorbic Acids on Electrodeposited Au/FeAu Multilayer Nanowires

S. Lucatero and E. J. Podlaha[*,z]

Chemical Engineering Department, Northeastern University, Boston, Massachusetts 02115, USA

AuFe electrodeposits onto a rotating disk electrode were examined to assess the composition and current efficiency behavior when citric acid, ascorbic acid, or a combination of both is present in the electrolyte. Nanowires were subsequently fabricated with pulsed current deposition to create compositionally, multilayered Au/FeAu nanowires. The FeAu layer of the nanowires was porous in a citrate electrolyte, but the porosity decreased with the addition of ascorbic acid in the electrolyte. Comparatively higher side reaction partial current densities (i_{sr}) in the citric acid electrolyte generated local alkaline conditions, inducing the chemical precipitation of Fe ions in the form of iron oxide nanoparticles inside the recess, which manifested as the regions of high porosity. Nonporous layers observed in the ascorbic acid bath, in combination with decreased i_{sr} and increased current efficiency of the deposits, suggested that a similar mechanism of Fe precipitation inside the nanorecess is less likely.
 [DOI: 10.1149/1.3409843]

Manuscript submitted February 8, 2010; revised manuscript received March 17, 2010. Published May 3, 2010.

Multilayered materials, tailored with repetitive sequences of magnetic segments interspaced by noble metal layers, display unique properties often superior to their elemental constituents. For example, the giant magnetoresistance (GMR)[1,2] and large magnetoimpedance[3,4] of multilayered thin films and nanowires[5-10] are of interest for magnetic recording heads, sensing applications, and remote communication devices. Variations in layer thickness provide a means to modulate their magneto-optical,[11,12] GMR, and related magnetic properties.[13] In particular, nanostructures composed of Fe layers sandwiched by thin films of Au [12,14-22] and AuFe alloys[16-19] show interesting magnetic characteristics and enhanced magneto-optical properties compared to those of pure Fe films[18,19] or bulk values.[23] A distinct feature of Au/Fe monatomic multilayers is the artificial formation of superlattices with an ordered structure and a ferromagnetic character.[12,20-25]

Electrodeposition constitutes a practical approach for the fabrication of both multilayered nanowire structures and thin film alloys.[5-10,26] In either case, the periodicity of current or applied potential pulses trigger alternate growth of the less noble (more noble) metal layer at low (high) values. These substrates can be subsequently etched to obtain nanoporous structures[27-33] of interest for a variety of applications, such as drug delivery.[34,35] The fabrication of multilayer nanowires with alternating porous (AuFe) and nonporous (Au) segments by single-step electrodeposition was recently reported by our group.[36] The deposition current density influenced the morphology of the fabricated structure in a citric acid electrolyte with relatively low current efficiency (2–10%). It was postulated that the low current efficiency contributed to the formation of porous regions within nanowires. In the work presented here, the effect of the complexing agent on current efficiency, composition, and porosity of the deposit is examined.

The choice of ligand must be compatible with both gold and iron ions for alloy reduction. Cyanide has been used as stabilizing species in many electroplating solutions, including Au.[27,28,37] The stability constant of the $[Au(CN)_2]^-$ complex is 10^{39},[37] whereas that of $Fe(CN)_6$ is 10^{35} for Fe^{2+};[38] however, the toxicity of the cyanide species are well known, and less harmful alternatives (i.e., citric and ascorbic acids) are considered in this work. Some complexants are particularly suitable for alloy synthesis, owing to their ability to bring two or more reduction potentials in close proximity, favoring a shift of potential. In addition, other complexants exhibit a tendency to reduce metal ions in the solution[39-43] and may favorably contribute to the efficiency of electrodeposition via an electroless plating process. The ability of citric acid to form stable interactions and strong complexes with noble and transition metals, together with its nontoxic nature, have made this ligand a popular choice for Au electrolytes and other plating solutions.[37,44-47] In addition to being a complexant, this ligand has been utilized for the chemical synthesis of Au nanoparticles, owing to its reducing properties.[48,49] However, ascorbic acid exhibits a strong reducing character toward noble and transition metals[50-55] and rather low complexing stability constants ($0.2 < \log K < 2.35$).[52,56-58] In this study, the electrodeposition conditions for Au–Fe thin films and Au/FeAu multilayer nanowires are compared in both citric and ascorbic acid electrolytes.

Experimental

Two different working electrodes were used: (*i*) a rotating cylinder electrode (RCE) and (*ii*) polycarbonate (PC) nanoporous membranes. The RCE was utilized to characterize the compositional dependence and efficiency of the deposits. These thin-film deposits were galvanostatically deposited in a cell with a copper RCE (6 cm length and 0.6 cm diameter), a stationary platinum mesh as the counter electrode, and a saturated calomel reference electrode (SCE). The experiments were performed at three different rotation rates, i.e., 200, 400, and 650 rpm, and the current density was varied in the range of -0.3 to -20 mA/cm^2. Polarization curves were performed at a sweep rate of 5 mV/s.

Nanowires deposited within track-etched PC membranes (6 μm thick and 100 nm pore diameter, Osmonics) were fabricated by a pulsing current between two cathodic potentials, resulting in multilayered structures. The noble metal layer was developed at $i_1 = -0.9$ mA/cm^2 ($t_1 = 135$ s) and the alloy segment at $i_2 = -10$ mA/cm^2 ($t_2 = 25$ s). The cathode consisted of the PC membrane sputtered on one side with Au and placed inside a poly ether ether ketone (PEEK) holder; a Au anode was aligned horizontally to the membrane and an SCE was used. Multilayers were deposited without agitation. The nanowires were released from the templates using a dichloromethane bath for 12 h; solvent removal was achieved by repeated dilution/centrifugation with high purity ethanol and ultrasonication.

The electrolytes contained 0.29 M $FeSO_4$, 1.07 M KOH, and 2.5 mM Au (Techni Gold 25 E) and a complexing additive: (*i*) 0.49 M citric acid, (*ii*) 0.245 M citric and 0.245 M ascorbic acids combined (1:1), or (*iii*) 0.49 M ascorbic acid. The pH was adjusted to 6.15 with diluted H_2SO_4 or KOH at room temperature, and deionized ultrafiltered water (Fisher Scientific) was utilized for all experiments. Solutions were prepared immediately before each experiment. Quantitative compositional analysis of the deposits and nanowires was conducted by X-ray fluorescence spectroscopy operating at 45 keV, 2 mA in air with a 100 μm collimeter.

Transmission electron microscopy (TEM) was used to characterize the multilayer nanowires; approximately 20 μL of the concentrated nanowire suspension was placed in a Cu/carbon-coated TEM grid and visualized under a JEOL 1010 transmission electron microscope operating at an accelerating voltage of 60 kV in bright field.

* Electrochemical Society Active Member.
[z] E-mail: e.podlaha-murphy@neu.edu

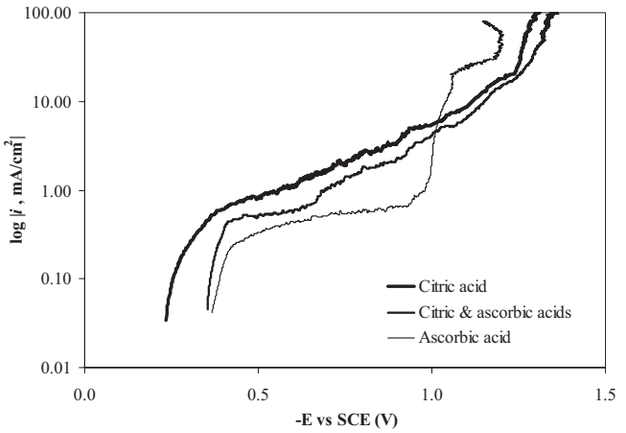

Figure 1. Alloy electrodeposition onto an RCE; effect of complexant species on the polarization behavior at 200 rpm.

Scanning electron microscopy (SEM) images were taken with the aid of a Hitachi S4800 field-emission-scanning electron microscope operated at 3.0 kV.

Porosity was quantitatively characterized by means of image analysis (Image J, NIH, Baltimore, MD). Processing of original 8 bit TEM files consisted of binary image reconstruction at a set gray-scale threshold (70–90). Approximately 100 in-focus segments were measured to obtain a representative porosity determination, which was calculated as the ratio of void area to total area.

Results and Discussion

RCE characterization.— The electrodeposition of AuFe alloys onto an RCE at different rotation rates and over a range of current density was performed with the purpose of defining pulsed current density conditions for the fabrication of Au/FeAu multilayer nanowires. The polarization curve in Fig. 1 shows the cathodic response when different complexing species (i.e., citric acid, ascorbic acid, and the combination of both citric and ascorbic acids) are present in the electrolyte at a constant working electrode rotation rate of 200 rpm. The polarization curves exhibited two distinct regions; a flat region near −0.4 V vs SCE was observed for all electrolytes, being the most pronounced in the ascorbic acid electrolyte, extending to −0.9 V. This region was indicative of Au deposition under mass-transport conditions because Au(I) ions are 2 orders of magnitude lower than Fe(II) ions in the electrolyte. The rise in current density with more negative potentials was associated with the deposition of the less noble species, Fe, predominantly under kinetic control. In this latter region, the ascorbic acid electrolyte showed a steeper slope than the citric acid solution or the electrolyte with the combined (1:1) citric and ascorbic acids, suggesting more facile reactions in the presence of only ascorbic acid. The combined (1:1) citric and ascorbic acid electrolytes exhibited a polarization curve falling between those generated for the solutions with either citric acid or ascorbic acid alone and, in general, an intermediate trend was observed.

In Fig. 2a and b, the alloy elemental composition is presented for the three different electrolytes at 200, 400, and 650 rpm. These results are consistent with the polarization curves, where at smaller absolute values of total current density, Au deposition is favored, whereas more negative values included Fe deposition with increasing concentration. The type of complexant in the electrolyte significantly influenced deposit composition; at the same current density, composites with higher Fe content (Fig. 2a) were obtained in the ascorbic acid electrolyte (solid curves, black filled symbols) compared to those obtained with either the citric acid solution (solid curves, white filled symbols) or in the electrolyte with citric and ascorbic acids combined (dotted curves, gray filled symbols). Deposit composition was also affected by the electrode rotation rate. In

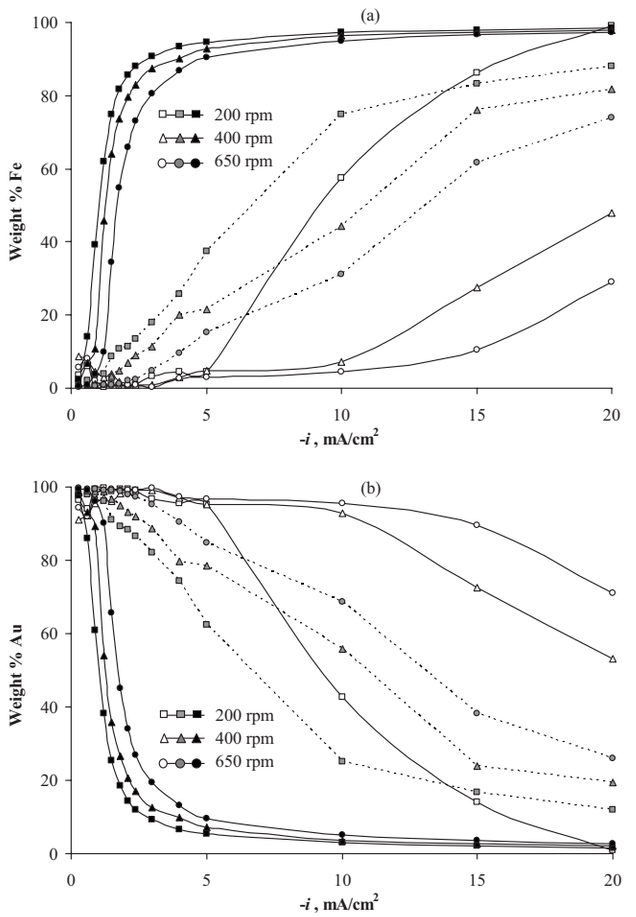

Figure 2. Effect of rotation rate and complexant on (a) wt % Fe and (b) wt % Au of deposits in the electrolyte with ascorbic acid (black filled symbols), citric acid (white filled symbols), and citric and ascorbic acids combined (1:1) (gray filled symbols).

all electrolytes, an increased (decreased) Au (Fe) content upon increasing rotation rate from 200 to 650 rpm is observed in Fig. 2b (Fig. 2a). This effect was more pronounced in the citric acid electrolyte than that observed in the ascorbic acid electrolyte.

Figure 3 presents the current efficiency during deposition with the three different electrolytes at electrode rotation rates of 200, 400, and 650 rpm. Values were calculated by dividing the experimentally determined deposited mass with the theoretically predicted value from Faraday's law. The type of complexing species had a dramatic effect on the current efficiency, significantly higher values were observed in the ascorbic acid electrolyte (~6 to 82%) compared to those generated by the citric acid solution (~2 to 10%). Intermediate efficiency values were observed in the electrolyte with a combination of citric and ascorbic acids. The influence of rotation rate on current efficiency had a small effect in either the citric acid solution or the ascorbic acid electrolyte and a more prominent influence when both citric and ascorbic acid were present together in the electrolyte. In the electrolytes with ascorbic acid, higher efficiencies were observed by decreasing the rotation rate between 200 and 650 rpm.

The deconvolution of the total current density is presented in Fig. 4, 7, and 8 as partial current densities of each metal species and side reactions using the composition data in Fig. 2a and b, measured deposit thickness and Faraday's law. The dependence of Au partial current density (i_{Au}) with the rotation rate and type of complexant at a steady state is shown in Fig. 4. Increased i_{Au} values with rotation rate were consistent with increased Au content in the deposits at

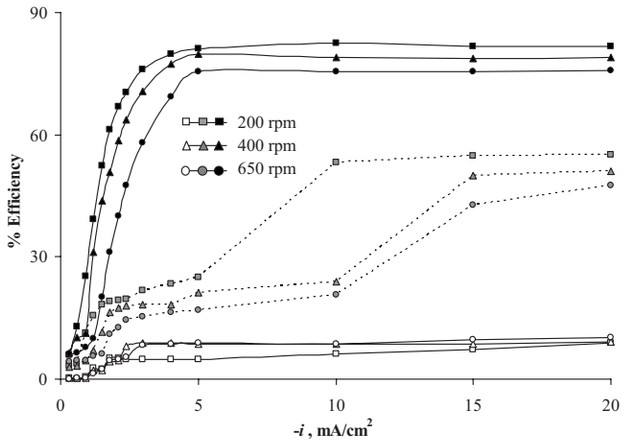

Figure 3. Current efficiency of Au–Fe electrodeposits as function of rotation rate and type of complexant species; electrolyte with ascorbic acid (black filled symbols), citric acid (white filled symbols), and citric and ascorbic acids combined (1:1) (gray filled symbols).

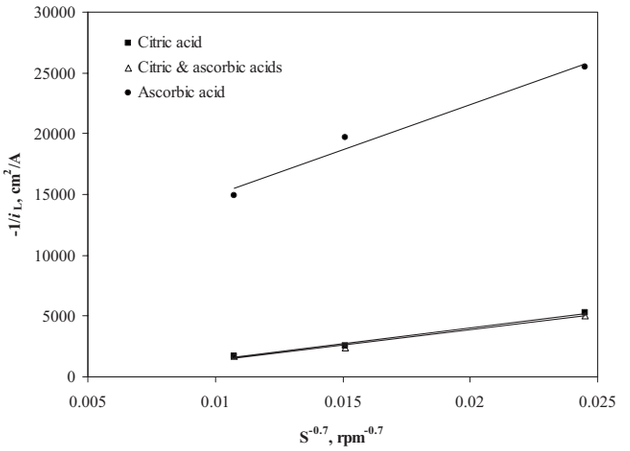

Figure 5. Dependence of the inverse gold limiting current density with rotation rate to the −0.7 power for different electrolytes.

large overpotentials. As previously noted in the first paragraph of the Results and Discussion section, this trend is expected due to its very low concentration (i.e., 2.5 mM) and mass-transport control. Particularly for the electrolyte with citric acid (Fig. 4), a kinetic regime can be distinguished at a low overpotential. The gold diffusion coefficient (D) for the three different electrolytes studied was estimated from the dependence of the limiting current density (i_L) with rotation rate (S) to the 0.7th power described by Eisenberg et al.[59] for an RCE system

$$i_L = 0.01nFC^b D^{0.644}\nu^{-0.344}S^{0.7}d_i^{0.4} \quad [1]$$

where n is the number of electrons transferred, F is Faraday's constant, C^b is the gold bulk concentration, ν is the kinematic viscosity (0.01 cm^2/s), and d_i is the cathode diameter. The i_{Au} limiting current density values (i_L) in Fig. 5 were extracted from Fig. 4. The limiting current density was clearly evident for the ascorbic acid electrolyte, characterized by a constant current response with potential over a wide range. In this electrolyte, the value of the limiting current density was averaged at potentials between −0.93 and 1.29 V (200 rpm), −0.97 and −1.28 V (400 rpm), and −0.8 and 1.27 V (650 rpm). The electrolyte with citric acid did not have a typical limiting current density behavior due to a decrease in current density at large, negative potentials. In this case, the i_L was interpolated near the maximum current density response. At 200, 400, and 650 rpm, these values were −0.91, −1.24, and −1.28 V, respectively; for the electrolyte with a combination of citric and ascorbic acids, i_{Au} values were estimated at 0.83 (200 rpm), 0.95 (400 rpm), and 1.15 V (650 rpm). Similar D values for the citric acid electrolyte and for that with a combination of citric and ascorbic acids (i.e., 4.5×10^{-6} and 4.9×10^{-6} cm^2/s, respectively) were calculated from the slopes in Fig. 5 and Eq. 1, whereas for the ascorbic acid solution, D was almost an order of magnitude lower, 9.1×10^{-7} cm^2/s. This decreased diffusion coefficient reflects a lower i_L value associated by a possible decrease in the bulk concentration of Au ions as a consequence of the formation of nanoparticles.

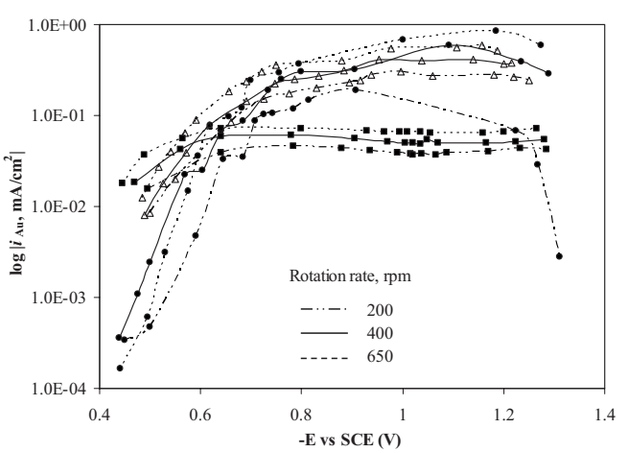

Figure 4. Partial current density of Au determined from RCE at 200, 400, and 650 rpm for the electrolyte with citric acid (●), citric and ascorbic acids combined (△), and ascorbic acid (■).

The electrolyte was analyzed by TEM to verify nanoparticle formation. Clumps composed of numerous nanoparticles (Fig. 6a) were found in the ascorbic acid electrolyte, whereas in the citric acid solution, no nanoparticles were observed, with the exception of only a few dispersed microsize particles. Nanoparticles, either dispersed or grouped together, were also seen in the electrolyte with citric and ascorbic acids combined (Fig. 6b); however, in this case, the diffusion coefficient was unaffected in relation to the citric acid solution, possibly by the ability of citric acid at maintaining the stability of Au ions.[37,45] The strong reducing properties of ascorbic acid are well documented[50-55] and have been explored in the determination of noble metals in aqueous solutions by titration[60-62] and for the chemical synthesis of Au nanoparticles with controlled morphological shape and dimensions.[39-43] The reduction of Au(III) to either Au(I) (E^0 = +1.36 V) or Au(0) (E^0 = +1.52 V) [63] and the simultaneous oxidation of ascorbic acid (E^0 = +0.06 V) [57,63] are thermodynamically favored. However, Fe^{3+} reduction to Fe^{2+} (E^0 = +0.771 V) [63] by ascorbic acid is believed to occur through a multistep mechanism involving the formation of Fe–ascorbate and other types of complexes as short-lived intermediates that further hydrolyze to dehydroascorbic acid and Fe(II).[55,56,64] However, the reduction of Fe^{2+} to Fe(s) is unlikely given the standard potential for this reaction (E^0 = −0.44).[63] These data suggest that nanoparticles that form in the bulk electrolytes must be Au rather than Fe-based.

Figure 7 shows the accompanying behavior of the partial current density of iron (i_{Fe}) with electrode rotation rate and type of complexant. In contrast to i_{Au} (Fig. 4), i_{Fe} values did not plateau at more cathodic potentials and were comparatively higher, as expected because the Fe(II) ion concentration (0.29 M) is much higher than the Au(I) ion concentration. The i_{Fe} gradually increased in a steeper fashion in the electrolytes containing ascorbic acid (Fig. 7), suggesting relatively facile kinetics of Fe deposition and showing consistency with increased efficiencies and Fe content in the deposits at current densities more negative than −1.2 mA/cm^2 (Fig. 2a and 3). In contrast, more sluggish kinetics is apparent from the decreased

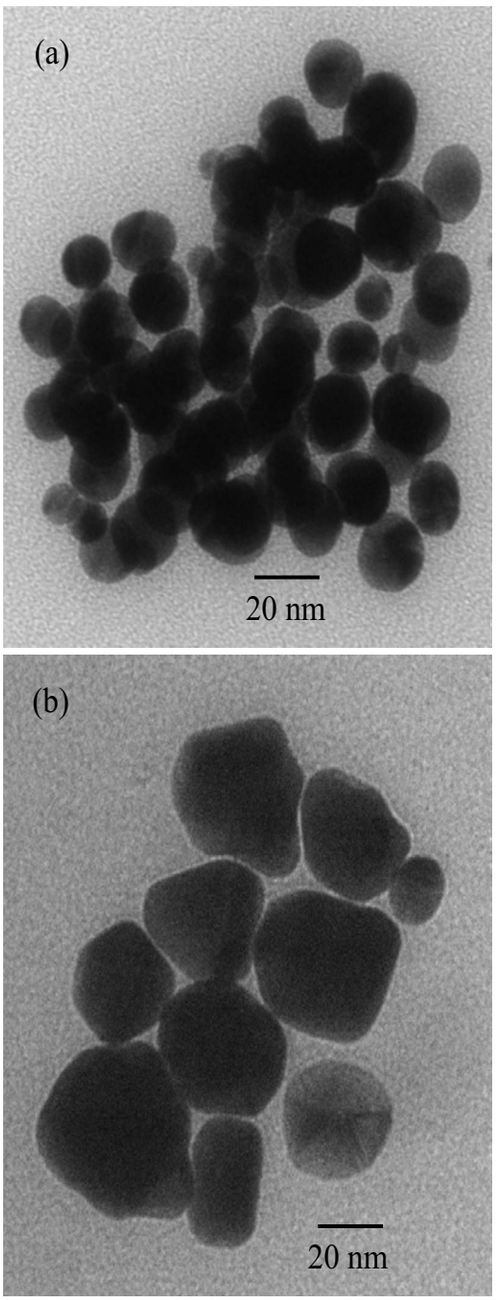

Figure 6. Nanoparticle formation in the electrolyte with (a) ascorbic acid and (b) citric and ascorbic acids combined.

slopes in the citric acid electrolyte (Fig. 7). Again, i_{Fe} values for the electrolyte added with a combination of citric and ascorbic acids (Fig. 7) fell in between those obtained for the electrolytes with a single complexant. With the exception of the citric acid electrolyte, at potentials less negative than −0.7 V, i_{Fe} was not significantly affected by rotation rate, indicating a kinetic control behavior. Table I compares the Fe charge-transfer coefficient (α_{Fe}) for all three different electrolytes, which was calculated from the slope of Tafel plots in the range of potential where kinetic deposition dominates (i.e., −0.8 to −1.3 V). All of the Tafel slopes in Table I were comparatively lower than that reported by Matlosz[65] for uncomplexed Fe (i.e., 70 V^{-1}, α_{Fe} = 1.79), suggesting, and agreeing with the literature,[38] that citric and ascorbic acids may both complex iron ions. Studies have demonstrated that ascorbic acid interacts with

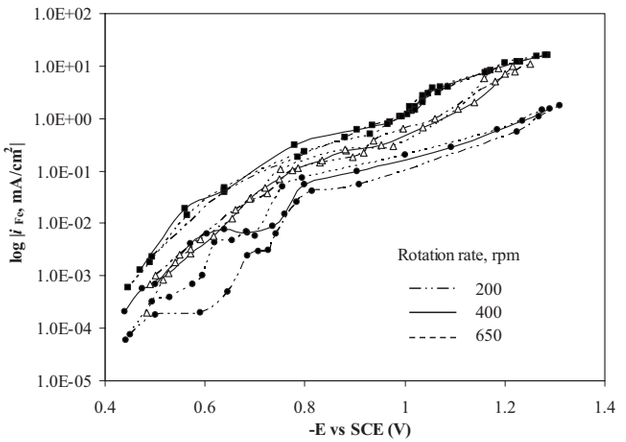

Figure 7. Partial current density of Fe determined from RCE at 200, 400, and 650 rpm for the electrolyte with citric acid (●), citric and ascorbic acids combined (△), and ascorbic acid (■).

iron forming intermediates of a transient nature[55,56,64] and also stabilizes complexes with Fe^{+3} and Fe^{+2}, likely through the oxygen atoms on the 2 and 3 carbons.[66,67] Citric acid exhibits slightly higher stability constant values with Fe^{+2} (log K_1 = 4.8, log K_2 = 2.9, and log K_3 = 1.1)[38] than the Fe–ascorbate complex (log K values range between 0.21 and 6.36),[38] which may explain the lower transfer coefficient with citric acid due to more Fe^{2+} complexed and slower kinetics with the complexed reactant. The mixed electrolyte has a similar α_{Fe} value as the ascorbic acid, suggesting the dominating influence of ascorbic acid. In addition to the more facile kinetics at more cathodic potentials observed in the presence of ascorbic acid (Table I), the fact that ascorbic acid is a strong reducing compound[50-55] was also consistent with increased i_{Fe} values (Fig. 7) and Fe content in the deposits (Fig. 2b).

Figure 8 plots the partial current density of side reactions (i_{sr}) for different electrolyte formulations at 200, 400, and 650 rpm. As opposed to the behavior of i_{Fe}, the lowest i_{sr} values were for the ascorbic acid electrolyte, whereas the citric acid electrolyte generated the highest i_{sr} values, suggesting a noticeable gas evolution in the latter solution. An effect of rotation rate on i_{sr} suggested gaseous evolution from hydrogen and water reduction at less and more negative potentials, respectively. Hydrogen generation by reduction of citrate has been noted as a reason of relatively low current efficiencies observed during NiMo alloy electrodeposition.[68] In the present study, the high i_{sr} values observed in the citric acid electrolyte in relation to the ascorbic acid-containing electrolytes (Fig. 8) suggest that a similar citrate reduction may cause current losses and consequently leads to low current efficiencies (Fig. 3).

Multilayer nanowire fabrication.— In a previous paper,[43] AuFe nanowires were electrodeposited from nanoporous membranes and the resulting structure was porous with the citric acid electrolyte. In the present study, the type of complexant species in the electrolyte also showed an effect on the porosity of nanowires. Figure 9 shows such effect on multilayers fabricated at $i_1 = -0.9$ mA/cm^2 (t_1 = 135 s) and $i_2 = -10.0$ mA/cm^2 (t_2 = 25 s) used to deposit a

Table I. Fe Tafel slopes and charge-transfer coefficient for different electrolytes calculated from Fig. 7.

Complexant species	Tafel slope (V^{-1})	α_{Fe}
Citric acid	6.8	0.17
Citric and ascorbic acids combined (1:1)	11.2	0.28
Ascorbic acid	10.6	0.27

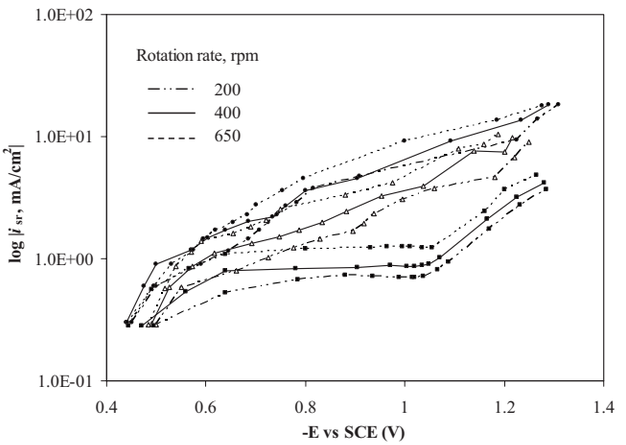

Figure 8. Partial current density of side reactions determined from RCE at 200, 400, and 650 rpm for the electrolyte with citric acid (●), citric and ascorbic acids combined (△), and ascorbic acid (■).

layer of Au and AuFe, respectively, using the (a) citric acid electrolyte, (b) the solution with both citric and ascorbic acids, and (c) with ascorbic acid only. A gradual decrease in porosity (ε) was estimated from quantitative image analysis upon replacing citric acid with ascorbic acid. Highly porous layers ($\varepsilon = 0.62$) were developed in the citric acid electrolyte (Fig. 9a), whereas completely solid, nonporous nanowires were synthesized in the ascorbic acid electrolyte, and only a modulation at the nanowire borders was observed (Fig. 9c). In the electrolyte with a combination of citric and ascorbic acids, denser layers ($\varepsilon = 0.35$) than in the citric acid solution were developed. The thickness of the AuFe layer deposited at $i_2 = -10.0$ mA/cm^2 ($t_2 = 25$ s) estimated from TEM imaging was 45 ± 10 nm in all three different electrolytes studied (Fig. 9), being consistent with a kinetic process dominating at such a current density. Instead of thicker porous layers with improved efficiency from the ascorbic acid and combination electrolytes, deposition within the pores generated denser (solid) layers. A thicker layer of high porosity may be expected for a process under mass-transport control, with the deposition occurring only at the developing interface. Coupled mechanisms of gas evolution and chemical formation of nanoparticles at the growing solid–liquid interface are believed to occur simultaneously and both may have been contributing factors in the development of highly porous multilayers in the citric acid electrolyte. As a consequence of the large side reaction occurring in the citrate electrolytes, local alkaline conditions could have been created at the developing interface inside the nanorecess, which in turn, may have favored the chemical formation of nanoparticles, and therefore layers with a porous structure. The synthesis of iron oxide nanoparticles by chemical precipitation of iron ions is known to occur in alkaline conditions in the presence[69] and absence of citric acid.[70-72] The postulated mechanism is less likely in the presence of ascorbic

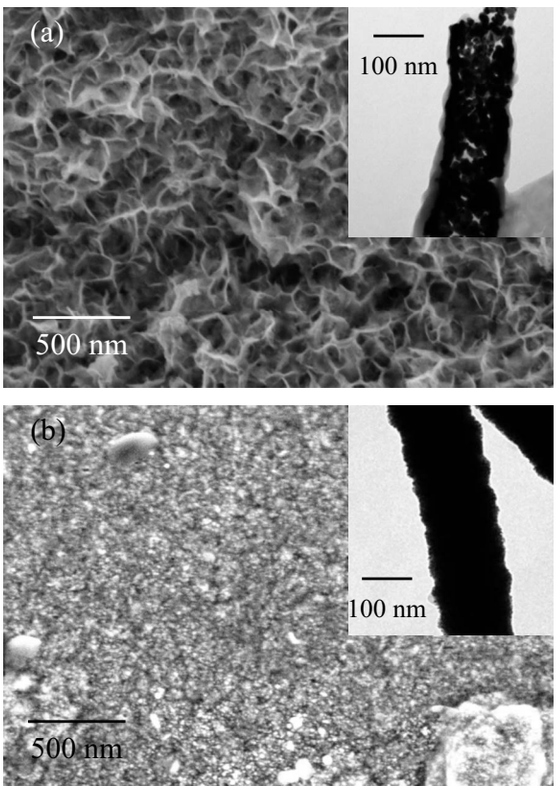

Figure 10. SEM images of RCE electrodeposits at $i = -10$ mA/cm^2 and 200 rpm in the electrolyte with (a) citric acid and (b) ascorbic acid. Insets show nanowires fabricated at i_1 (t_1) = 0.0 mA/cm^2 (135 s) and i_2 (t_2) = −10.0 mA/cm^2 (25 s) in the respective electrolytes.

acid because decreased i_{sr} values were observed in this electrolyte (Fig. 8), suggesting that the water reduction reaction and the local alkalinity may have evolved to a significantly lower extent, with the net result of a total absence of porosity. Also, local alkalinity generated by hydrogen evolution in all electrolytes would be unfavorable for the formation of Au nanoparticles by chemical reduction because this process preferably occurs at acidic or neutral conditions.[41,55,60]

Figure 10 shows the SEM images of RCE electrodeposits obtained at the current density conditions for the alloy layer ($i_2 = -10$ mA/cm^2) and 200 rpm and nanowires fabricated at $i_1 = 0.0$ mA/cm^2 ($t_1 = 135$ s) and $i_2 = -10$ mA/cm^2 ($t_2 = 25$ s) in the electrolytes with (a) citric acid and (b) ascorbic acid. A dendritic appearance of the deposit in Fig. 10a contrasts with the solid aspect of that in Fig. 10b, suggesting that gas formation and a rise in local alkalinity may also be present at a larger scale. At such pulsed current conditions, no deposition occurs at $i_1 = 0.0$ mA/cm^2 (t_1

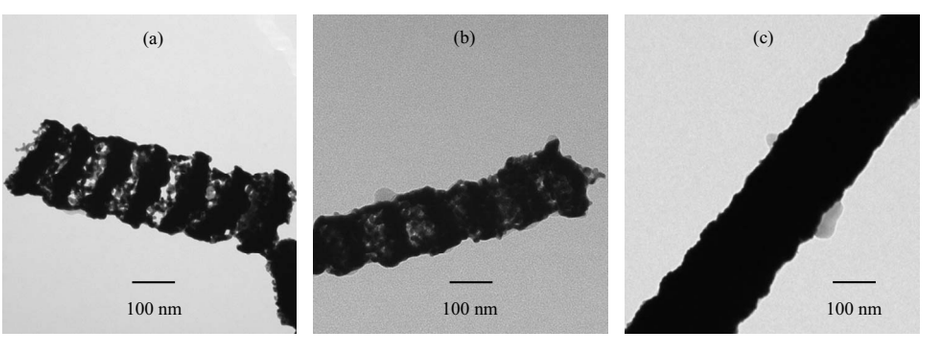

Figure 9. Effect of complexant on multilayer porosity, (a) citric acid, (b) citric-ascorbic, and (c) ascorbic acid; i_1 (t_1) = −0.9 mA/cm^2 (135 s) and i_2 (t_2) = −10.0 mA/cm^2 (25 s) for (a) and (b), respectively.

= 135 s); consequently, completely porous nanowires were observed in the citric acid electrolyte, whereas again, solid layers developed in the ascorbic acid solution, consistent with the increased efficiency in the ascorbic acid electrolyte (Fig. 3). At the current conditions for the porous layer, i.e., $i_2 = -10$ mA/cm^2 and $t_2 = 25$ s, Fe content and efficiency of electrodeposits at 200 rpm was equal to 57 and 6%, respectively, in the citric acid electrolyte. Both values increased to 75% (Fe content) and 53% (efficiency) in the electrolyte with a combination of citric and ascorbic acids, and the highest efficiency and Fe content were observed in the ascorbic acid electrolyte (97 and 82%, respectively). However, Au-rich layers deposited at the low current pulse (i.e., $i_1 = -0.9$ mA/cm^2) did not show porosity in any of the three electrolytes, chiefly because at such a low current density, gas evolution was minimal.

Conclusions

The type of complexant species affected the deposition behavior of the binary Au–Fe electrolyte and the characteristics of the Au/FeAu multilayer nanowires. At the same applied current density and pulse time, nanowires with dense layers developed in the electrolytes with ascorbic acid compared with porous segments observed in the citric acid solution. Comparatively low efficiencies (~2 to 10%) and an increased partial current density of side reactions in the latter bath were responsible for a porous structure. The local alkalinity favors the chemical formation of iron nanoparticles inside the recess and is incorporated into the deposit, providing a scaffold for a porous structure. In the ascorbic acid electrolyte, more facile kinetics and increased efficiencies minimized the chemical formation of iron oxide nanoparticles with respect to the citric acid electrolyte and prevented the porous morphology, although in the bulk electrolyte, Au nanoparticles were formed, as reflected in a lower effective Au diffusion coefficient.

Acknowledgments

The authors thank the National Science Foundation (CBET no. 0746567) for support of this work. Assistance with SEM and TEM imaging from W. H. Fowle is greatly appreciated.

Northeastern University assisted in meeting the publication costs of this article.

References

1. W. Schwarzacher and D. Lashmore, *IEEE Trans. Magn.*, **32**, 3133 (1996).
2. A. Fert, A. Barthélémy, P. Galtier, P. Holody, R. Loloee, R. Morel, F. Pétroff, P. Schroeder, L. B. Steren, and T. Valet, *Mater. Sci. Eng., B*, **31**, 1 (1995).
3. D. P. Makhnovskiy, N. Fry, L. V. Panina, and D. J. Mapps, *J. Appl. Phys.*, **96**, 2150 (2004).
4. D. de Cos, N. Fry, I. Orue, L. V. Panina, A. Garcia-Arribas, and J. M. Barandiaran, *Sens. Actuators, A*, **129**, 256 (2006).
5. D. Pullini, D. Busquets, A. Ruotolo, G. Innocenti, and V. Amigó, *J. Magn. Magn. Mater.*, **316**, e242 (2007).
6. W. Schwarzacher, O. I. Kasyutich, P. R. Evans, M. G. Darbyshire, G. Yi, V. M. Fedosyuk, F. Rousseaux, E. Cambril, and D. Decanini, *J. Magn. Magn. Mater.*, **198–199**, 185 (1999).
7. A. Blondel, J. P. Meier, B. Doudin, and J.-Ph. Ansermet, *Appl. Phys. Lett.*, **65**, 3019 (1994).
8. F. Nasirpouri, P. Southern, M. Ghorbani, A. Iraji zad, and W. Schwarzacher, *J. Magn. Magn. Mater.*, **308**, 35 (2007).
9. G. P. Heydon, S. R. Hoon, A. N. Farley, S. L. Tomlinson, M. S. Valera, K. Attenborough, and W. Schwarzacher, *J. Phys. D*, **30**, 1083 (1997).
10. L. Piraux, J. M. George, J. F. Despres, C. Leroy, E. Ferain, R. Legras, K. Ounadjela, and A. Fert, *Appl. Phys. Lett.*, **65**, 2484 (1994).
11. W. Geerts, Y. Suzuki, T. Katayama, K. Tanaka, K. Ando, and S. Yoshida, *Phys. Rev. B*, **50**, 12581 (1994).
12. K. Sato, E. Takeda, M. Akita, M. Yamaguchi, K. Takanashi, S. Mitani, H. Fujimori, and Y. Suzuki, *J. Appl. Phys.*, **86**, 4985 (1999).
13. L. Sun, Y. Hao, C.-L. Chien, and P. C. Searson, *IBM J. Res. Dev.*, **49**, 79 (2005).
14. Y. Suzuki, T. Katayama, S. Yoshida, K. Tanaka, and K. Sato, *Phys. Rev. Lett.*, **68**, 3355 (1992).
15. T. Katayama, H. Awano, and N. Koshizuka, *J. Phys. Soc. Jpn.*, **55**, 2539 (1986).
16. S. Mitani, K. Takanashi, H. Nakajima, K. Sato, R. Schreiber, P. Grünberg, and H. Fujimori, *J. Magn. Magn. Mater.*, **156**, 7 (1996).
17. Y. Kobayashi, S. Nasu, T. Emoto, and T. Shinjo, *Physica B*, **237–238**, 249 (1997).
18. K. W. Kim, Y. H. Hyun, R. Gontarz, Y. V. Kudryavtsev, and Y. P. Lee, *Phys. Status Solidi A*, **196**, 197 (2003).
19. Y. P. Lee, Y. H. Hyun, Y. V. Kudryavtsev, and R. Gontarz, *J. Funct. Mater.*, **10**, 3 (2003).
20. L. Uba, S. Uba, V. N. Antonov, A. N. Yaresco, T. Ślezak, and J. Korecki, *Phys. Rev. B*, **62**, 13731 (2000).
21. Z.-P. Shi, J. F. Cooke, Z. Zhang, and B. M. Klein, *Phys. Rev. B*, **54**, 3030 (1996).
22. S. Riedling, N. Knorr, C. Mathieu, J. Jorzick, S. O. Demokritov, B. Hillebrands, R. Schreiber, and P. Grünberg, *J. Magn. Magn. Mater.*, **198–199**, 348 (1999).
23. G. S. Krinchik and B. A. Artem'ev, *Sov. Phys. JETP*, **26**, 1080 (1968).
24. K. Takanashi, S. Mitani, M. Sano, H. Fujimori, H. Nakajima, and A. Osawa, *Appl. Phys. Lett.*, **67**, 1016 (1995).
25. K. Takanashi, S. Mitani, K. Himi, and H. Fujimori, *Appl. Phys. Lett.*, **72**, 737 (1998).
26. Q. Huang and E. J. Podlaha, *J. Electrochem. Soc.*, **151**, C119 (2004).
27. C. X. Ji and P. C. Searson, *J. Phys. Chem. B*, **107**, 4494 (2003).
28. C. X. Ji and P. C. Searson, *Appl. Phys. Lett.*, **81**, 4437 (2002).
29. A. J. Forty, *Nature (London)*, **282**, 597 (1979).
30. J. Erlebacher, M. J. Aziz, A. Karma, N. Dimitrov, and K. Sieradzki, *Nature (London)*, **410**, 450 (2001).
31. H. W. Pickering and C. Wagner, *J. Electrochem. Soc.*, **114**, 698 (1967).
32. H. W. Pickering, *J. Electrochem. Soc.*, **115**, 143 (1968).
33. H. W. Pickering, *J. Electrochem. Soc.*, **115**, 690 (1968).
34. S. M. Cohen, *Curr. Opin. Chem. Biol.*, **11**, 115 (2007).
35. P. Horcajada, C. Serre, M. Vallet-Regí, M. Sebban, F. Taulelle, and G. Férey, *Angew. Chem., Int. Ed.*, **45**, 5974 (2006).
36. S. Lucatero, W. H. Fowle, and E. J. Podlaha, *Electrochem. Solid-State Lett.*, **12**, D96 (2009).
37. Y. Okinaka and M. Hoshino, *Gold Bull.*, **31**, 3 (1998).
38. NIST critically selected stability constants of metal complexes, data collected and selected by R. M. Smith and A. E. Martell, program developed by R. J. Motekaitis, National Institute of Standards and Technology, Standard Reference Data Program, Gaithersburg, MD (2001).
39. D. Andreescu, T. K. Sau, and D. V. Goia, *J. Colloid Interface Sci.*, **249**, 1870 (2005).
40. M. N. Nadagouda and R. S. Varma, *Cryst. Growth Des.*, **7**, 2582 (2007).
41. A. Murugadoss, R. Pasricha, and A. Chattopadhyay, *J. Colloid Interface Sci.*, **311**, 303 (2007).
42. M. Liu and P. Guyot-Sionnest, *J. Phys. Chem. B*, **108**, 5882 (2004).
43. Y. Khalavka, J. Becker, and C. Sönnichsen, *J. Am. Chem. Soc.*, **131**, 1871 (2009).
44. S. Rode, C. Henninot, C. Vallières, and M. Matlosz, *J. Electrochem. Soc.*, **151**, C405 (2004).
45. S. L. Cumberland and G. F. Strouse, *Langmuir*, **18**, 269 (2002).
46. E. Chassaing, N. Portail, A.-F. Levy, and G. Wang, *J. Appl. Electrochem.*, **34**, 1085 (2004).
47. A. Lozano-Morales, J. Fitzgerald, V. Singh, X. Xie, and E. J. Podlaha, *J. Electrochem. Soc.*, **153**, C567 (2006).
48. J. Cao, X. Hu, Z. Jiang, and Z. Xiong, *e-J. Surf. Sci. Nanotechnol.*, **7**, 134 (2009).
49. G. Frens, *Nature (London), Phys. Sci.*, **241**, 20 (1973).
50. R. W. Herbert, E. L. Hirst, E. G. V. Percival, R. J. W. Reynolds, and F. Smith, *J. Chem. Soc.*, **299**, 1270 (1933).
51. B. H. J. Bielski, in *Chemistry of Ascorbic Acid Radicals*, P. A. Seib and B. M. Tolbert, Editors, Advances in Chemistry Series no. 200, pp. 81–100, American Chemical Society, Washington, DC (1982).
52. A. E. Martell, in *Chelates of Ascorbic Acid: Formation and Catalytic Properties*, P. A. Seib and B. M. Tolbert, Editors, Advances in Chemistry Series no. 200, pp. 152–178, American Chemical Society, Washington, DC (1982).
53. C. Creutz, *Inorg. Chem.*, **20**, 4449 (1981).
54. J. E. Gorman and F. M. Clydesdale, *J. Food Sci.*, **48**, 1217 (1983).
55. M. B. Davies, *Polyhedron*, **11**, 285 (1992).
56. A. E. Martell, in *Ascorbic Acid: Its Chemistry, Metabolism and Uses*, Chap. 7, P. A. Seib and B. M. Tolbert, Editors, Advances in Chemistry Series, American Chemical Society, Washington, DC (1982).
57. B. Zümreoglu-Karan, *J. Nanopart. Res.*, **11**, 1099 (2009).
58. B. Zümreoglu-Karan, *Coord. Chem. Rev.*, **250**, 2295 (2006).
59. M. Eisenberg, C. W. Tobias, and C. R. Wilke, *J. Electrochem. Soc.*, **101**, 306 (1954).
60. L. Erdey and G. Siposs, *Fresenius' Z. Anal. Chem.*, **157**, 166 (1957).
61. S. N. Joshi, A. G. Kulkarni, and G. S. Deshmukh, *Anal. Chim. Acta*, **167**, 399 (1985).
62. T. Pal and P. K. Das, *Anal. Lett.*, **21**, 2333 (1988).
63. *Standard Potentials in Aqueous Solution*, A. J. Bard, R. Parsons, and J. Jordan, Editors, Marcel Dekker, NY (1985).
64. J. Xu and R. B. Jordan, *Inorg. Chem.*, **29**, 4180 (1990).
65. M. Matlosz, *J. Electrochem. Soc.*, **140**, 2272 (1993).
66. P. Martinez and D. Uribe, *Z. Naturforsch. B*, **37B**, 1446 (1982).
67. *Transition Metals in Biology and Their Coordination Chemistry*, W. Jabs, G. Krüger, A. X. Trautwein, V. Schünemann, and E. Bill, Editors, p. 468, John Wiley & Sons, Weinheim (1997).
68. E. Chassaing, K. Vu Quang, and R. Wiart, *J. Appl. Electrochem.*, **19**, 839 (1989).
69. Z. Ma, D. Dosev, M. Nichkova, R. K. Dumas, S. J. Gee, B. D. Hammock, K. Liu, and I. M. Kennedy, *J. Magn. Magn. Mater.*, **321**, 1368 (2009).
70. M. Chastellain, A. Petri, and H. Hofmann, *J. Colloid Interface Sci.*, **278**, 353 (2004).
71. C.-W. Hung, T. R. P. Holoman, P. Kofinas, and W. E. Bentley, *Biochem. Eng. J.*, **38**, 164 (2008).
72. M. Ma, Y. Zhang, W. Yu, H.-Y. Shen, H.-Q. Zhang, and N. Gu, *Colloids Surf., A*, **212**, 219 (2003).